Evaluating Late Cretaceous OAEs and the influence of marine incursions on organic carbon burial in an expansive East Asian paleo-lake

Matthew M. Jones[a,*], Daniel E. Ibarra[b], Yuan Gao[c], Bradley B. Sageman[a], David Selby[d], C. Page Chamberlain[b], Stephan A. Graham[e]

[a]Department of Earth and Planetary Sciences, Northwestern University, Evanston, Illinois 60208, USA matthewjones2012@u.northwestern.edu, b-sageman@northwestern.edu

[b]Department of Earth System Science, Stanford University, Stanford, California 94305, USA danieli@stanford.edu, chamb@stanford.edu

[c]State Key Laboratory of Biogeology and Environmental Geology, School of Earth Sciences and Resources, China University of Geosciences, Beijing, China yuangao@cugb.edu.cn

[d]Department of Earth Sciences, Durham University, Durham, DH1 3LE, UK david.selby@durham.ac.uk

[e]Department of Geological Sciences, Stanford University, Stanford, California 94305, USA sagraham@stanford.edu

*Corresponding author e-mail: matthewjones2012@u.northwestern.edu

Submitted to *Earth and Planetary Science Letters*
Category: Letter

Abstract

Expansive Late Cretaceous lacustrine deposits of East Asia offer unique stratigraphic records to better understand regional responses to global climate events, such as oceanic anoxic events (OAEs), and terrestrial organic carbon burial dynamics. This study presents bulk organic carbon isotopes ($\delta^{13}C_{org}$), elemental concentrations (XRF), and initial osmium ratios ($^{187}Os/^{188}Os$, Os_i) from the Turonian-Coniacian Qingshankou Formation, a ~5 Ma lacustrine mudstone succession in the Songliao Basin of northeast China. A notable $\delta^{13}C_{org}$ excursion (~+2.5‰) in organic carbon-lean Qingshankou Members 2-3 correlates to OAE3 in the Western Interior Basin (WIB) of North America within temporal uncertainty of high-precision age models. Decreases in carbon isotopic fractionation ($\Delta^{13}C$) through OAE3 in the WIB and Songliao Basin, suggest that significantly elevated global rates of organic carbon burial drew down pCO_2, likely cooling climate. Despite this, Os_i chemostratigraphy demonstrates no major changes in global volcanism or weathering trends through OAE3. Identification of OAE3 in a lake system is consistent with lacustrine records of other OAEs (e.g., Toarcian OAE), and underscores that terrestrial environments were sensitive to climate perturbations associated with OAEs. Additionally, the relatively radiogenic Os_i chemostratigraphy and XRF data confirm that the Qingshankou Formation was deposited in a non-marine setting. Organic carbon-rich intervals preserve no compelling Os_i evidence for marine incursions, an existing hypothesis for generating Member 1's prolific petroleum source rocks. Based on our results, we present a model for water column stratification and source rock deposition independent of marine incursions, detailing dominant biogeochemical cycles and lacustrine organic carbon burial mechanisms.

1. Introduction

Upper Cretaceous marine strata preserve evidence for greenhouse warmth on a planet with high pCO_2 (e.g., Pagani et al., 2014) and lacking sustained ice sheets (MacLeod et al., 2013). Oceanic anoxic events (OAEs) are superimposed on this stratigraphic record of excessive warmth, as relatively brief intervals (<1 Ma) of enhanced organic carbon burial in many basins globally (Jenkyns, 2010 and refernces therein) accompanied by positive stable carbon isotope excursions (CIEs) (Scholle and Arthur, 1980). Precise correlations of terrestrial and marine records are critical for developing a unified Late Cretaceous paleoclimate reconstruction and understanding the terrestrial response to OAEs, as well as for testing hypotheses for the causal mechanisms of OAEs. However, such correlations are complicated in terrestrial basins due to the common occurrence of hiatuses, lateral heterogeneity in lithofacies, and limited biostratigraphic age control. Despite challenges, some workers have employed carbon isotope ($\delta^{13}C$) chemostratigraphy to identify Mesozoic OAEs in terrestrial strata and assess local paleoclimate responses (e.g., OAE2, Barclay et al., 2010; OAE1a, Ludvigson et al., 2010). Although comparatively rare in the geologic record, lacustrine facies offer promise in reconstructing robust terrestrial paleoclimate records given relatively continuous, expanded mudstone successions. Paleo-lakes are also suitable for testing hypotheses about OAEs' triggering mechanisms, such as accelerated weathering, and for better resolving regional environmental responses (e.g., Toarcian OAE: Xu et al., 2017).

In the non-marine Songliao Basin of northeast China, the SK1-S core provides a relatively continuous Late Cretaceous stratigraphic record from lacustrine and fluvial units influenced by local tectonic and climatic conditions (Fig. 1) (Wang et al., 2013). In addition, the organic carbon-rich mudstones of the Turonian-Coniacian Qingshankou Member 1 are primary

petroleum source rocks in China's largest and longest producing non-marine oil and gas basin (Feng et al., 2010). As a result, the depositional history of the Qingshankou Formation has been heavily studied and debated, with some authors arguing that episodic incursions of marine waters during Member 1 drove water column stratification in the basin creating conditions favorable to preservation of organic carbon (e.g., Hou et al., 2000). More recently, the sporadic presence of biomarkers typical of marine algae and sponges in Member 1 and lowermost Members 2 and 3 (Hu et al., 2015), and pyrite sulfur isotopic records in Member 1 of SK1-S (Huang et al., 2013) have been interpreted as evidence for transient or even prolonged marine connections. However, the marine incursion hypothesis for source rock deposition in Qingshankou Member 1 remains controversial, as paleogeographic reconstructions note considerable distances to the nearest marine waters (>500 km; Yang, 2013) (Fig. 1) and because no well-preserved uniquely marine micro- or macro-fossils have been reported from the Qingshankou Formation in SK1-S (Xi et al., 2016). Others have interpreted a consistently non-marine water body during the deposition of the Qingshankou Formation (Chamberlain et al., 2013).

To assess the influence of OAEs and marine incursions on lacustrine organic carbon burial rates in the dominantly terrestrial Songliao Basin (Wang et al., 2016a), we present sedimentary geochemical measurements of the expanded mudstones of the Qingshankou Formation. The new mid-Turonian to late-Coniacian $\delta^{13}C_{org}$ records (*this study*; Hu et al., 2015) serve as a test of $\delta^{13}C_{org}$ correlation robustness from an East Asian lacustrine basin to the epicontinental marine $\delta^{13}C_{org}$ in the North American Western Interior Basin (WIB) (Joo and Sageman, 2014). Utilizing recently updated radioisotopic and astrochronologic age models (Locklair and Sageman, 2008; Wu et al., 2013; Sageman et al., 2014b; Wang et al., 2016b), we identify the Coniacian Oceanic

Anoxic Event 3 (OAE3) in Qingshankou Members 2 and 3 and investigate the event in a lake system using geochemical proxies.

Coupled with $\delta^{13}C$ chemostratigraphy, we present an initial osmium isotope ($^{187}Os/^{188}Os$ denoted as Os_i) chemostratigraphy from the Songliao Basin to test the marine incursion hypothesis. The Os_i data serve as a proxy for marine connectivity and basin restriction (e.g., Du Vivier et al., 2014), since values reflect a mixture of osmium derived from relatively homogenized open marine waters (Gannoun and Burton, 2014), mixing over geologically brief intervals (τ<10 ka, Oxburgh, 2001; Rooney et al., 2016), and local continental weathered osmium which tends to be more radiogenic (higher Os_i) (Peucker-Ehrenbrink and Ravizza, 2000). As a result, lacustrine formations, isolated from the marine osmium reservoir, generally preserve higher Os_i values due to the flux of proximal radiogenic osmium and limited unradiogenic osmium fluxes (e.g., cosmogenic dust and hydrothermal sources) (Poirier and Hillaire-Marcel, 2011; Cumming et al., 2012; Xu et al., 2017), with the caveat that lacustrine basins weathering ophiolitic lithologies preserve more unradiogenic Os_i (Kuroda et al., 2016). Thus, typical basins with a history of marine connections should record more non-radiogenic Os_i when compared to contemporaneous lacustrine basins. To constrain open marine Os_i values during deposition of Qingshankou Member 1, we present time correlative records from Turonian mudstones from the tropical North Atlantic. Furthermore, we interpret Os_i records as one proxy for continental weathering intensity through Qingshankou Members 2 and 3 (OAE3 interval as demonstrated by this study) and other intervals of SK1-S lacking additional evidence for marine incursions. Finally, to characterize marine osmium cycling and potential perturbations across OAE3 (e.g., LIP volcanism, continental weathering), we present a third small Os_i sample set from the Angus Core in the WIB (Denver Basin, Colorado).

Additionally, we present trace element (XRF) analyses spanning the Qingshankou Formation to reconstruct bottom-water redox conditions through major events in the lake's evolution, such as source rock deposition in Member 1 and OAE3 in Members 2 and 3, using established interpretive frameworks (Tribovillard et al., 2006; Sageman et al., 2014a). To conclude, we propose a depositional model, independent of marine connections, to characterize lacustrine biogeochemical cycling during accumulation of the Qingshankou Formation. This model provides a footing for future research to further evaluate scenarios for water column stratification and organic carbon deposition in mid-latitude paleo-lakes discussed herein.

2. Geologic materials SK1-S core

The terrestrial Songliao Basin in northeast China preserves a long-lived Jurassic-Cretaceous stratigraphic record in a deep (>5 km) backarc rifted sag basin (Fig. 1) (Graham et al., 2001; Wang et al., 2013; Wang et al., 2016a). An International Continental Drilling Project coring campaign recovered a sedimentary succession spanning the mid-Turonian to Campanian in two overlapping cores (SK1-S and SK1-N) in 2009. Three fluvio-deltaic formations (oldest to youngest: Quantou, Yaojia, Sifangtai) separated by two thick lacustrine formations (Qingshankou, Nenjiang) comprise the succession. A chronostratigraphic framework has been developed for SK1-S based on lithostratigraphy (Gao et al., 2009; Wang et al., 2009), and biostratigraphy of ostracod, charophyte, and, in the lower Nenjiang Formation, foraminifera (Wan et al., 2013; Xi et al., 2016). Recently published high-precision zircon U-Pb dates (Wang et al., 2016b) and astrochronology (Wu et al., 2013) in the Turonian-Coniacian Qingshankou Formation, the stratigraphic focus of this study, provide precise temporal constraints (±181 ka) necessary for global correlation and the interpretation of proxy data in the context of global climate events such as OAEs. The Qingshankou Formation is sub-divided into the lower 93m-

thick organic-rich laminated mudstone in Member 1 (Gao et al., 2009) and the upper 395m-thick undifferentiated grey shales of Members 2 and 3 (Wang et al., 2009).

3. Methods

3.1 Sampling and SK1-S timescale

We collected samples from SK1-S for this study at roughly 5-10 m spacing through the upper Quantou, Qingshankou, and lower Yaojia formations from the China University of Geosciences Beijing core repository. For all Qingshankou Formation samples analyzed, we assign numerical ages by anchoring the floating astronomical time scale from SK1-S (Wu et al., 2013) to a CA-ID-TIMS U/Pb zircon dated bentonite horizon (Ash S1705m = 90.97±0.12 Ma; Wang et al., 2016b) (Table A.1). Considering radioisotopic and astrochronologic sources of uncertainty, we calculate ±181 ka (2σ) precision for the anchored SK1-S time scale (see Appendix for detailed discussion).

3.2 Carbon geochemistry

We measured samples collected from the SK1-S Core for bulk organic carbon isotope ratios ($\delta^{13}C_{org}$), atomic carbon to nitrogen ratios (C/N), weight percent total organic carbon (TOC), and weight percent carbonate at Northwestern University (Appendix). Additionally, we measured a sample set from the Angus Core in the WIB for bulk carbonate carbon isotopes ($\delta^{13}C_{carb}$) to calculate $\Delta^{13}C$ ($\delta^{13}C_{carb}$-$\delta^{13}C_{org}$) to approximate changes in carbon isotope fractionation across OAE3 and compare to $\Delta^{13}C$ in the Songliao Basin (Appendix).

3.3 X-ray fluorescence (XRF)

Methods outlined in the Appendix are used to measure major and minor trace element concentrations of sample powders.

154 *3.4 Initial osmium isotope analysis*

155 To measure hydrogenous Os_i values, we analyzed ten samples from the Qingshankou
156 Formation on a Thermo Scientific Triton thermal ionization mass spectrometer at Durham
157 University via the established procedures of Selby and Creaser (2003) (see Appendix). We
158 selected samples in Member 1 and lowermost Members 2 and 3 from horizons proposed to
159 record biomarker evidence for marine incursions (Hu et al., 2015). Additionally, we analyzed
160 samples from the Turonian-aged black shales of Site 1259 at Demerara Rise (Tropical North
161 Atlantic ODP Leg 207) and Coniacian OAE3 interval in the Angus Core from the WIB. We
162 present these sample sets to characterize open and epicontinental marine Os_i values, respectively,
163 for comparison with the coeval Qingshankou Formation record and to test the hypothesis of
164 marine incursions into the Songliao Basin. To correct for post-depositional ^{187}Re decay to ^{187}Os
165 (see Appendix), we assign numerical ages to samples using an age model at Demerara Rise
166 (updated from Bornemann et al., 2008) and the existing Angus Core (Joo and Sageman, 2014)
167 and SK1-S age models (Sect. 3.1).

168 **4. Results**

169 *4.1 Bulk carbon chemistry TOC, C/N trends*

170 Weight percent TOC decreases upcore within the Qingshankou Formation from
171 maximum values in the laminated Member 1, consistently above 2% and up to ~8% TOC, to
172 values in Members 2 and 3 that rarely exceed 1% TOC. In TOC-rich Member 1, C/N ratios are
173 elevated (C/N = 8.5-25.6) above typical lacustrine algal values (C/N<8; Meyers, 1994) (Fig. 2;
174 see Table A.1). Occasionally, discrete horizons in Members 2 and 3 record elevated TOC spikes
175 punctuating the background pattern of decaying TOC levels. These horizons are accompanied
176 by increased C/N and enriched $\delta^{13}C_{org}$, with C/N (C/N = 15-25) approaching land-based vascular

plant organic matter values (C/N>25; Meyers, 1994) above the background lacustrine algal organic matter values. Additionally, new percent carbonate values are low, yet detectable throughout the studied interval (median=6.9%, max=22.5%) from scattered ostracods (Chamberlain et al., 2013; Wan et al., 2013).

4.2 Carbon isotopes

Bulk organic carbon isotope values in the studied interval are highly variable (-24 to -32.5‰) (Fig. 2; Table A.1-2). Some of this variability corresponds to changing facies, such as comparatively enriched $\delta^{13}C_{org}$ in fluvial facies of the Quantou and Yaojia Formations (generally $\delta^{13}C_{org} > -27‰$). However, lacustrine $\delta^{13}C_{org}$ values are also highly variable. Samples from Qingshankou Member 1 are strongly depleted in bulk $\delta^{13}C_{org}$, with an average value of -30.61‰ (1σ SD=±1.33‰) and minimum of -32.4‰. Interestingly, the bulk $\delta^{13}C_{org}$ of Member 1 is more depleted than both average Cretaceous marine (-27 to -29‰) and terrestrial (-24 to -25‰) end members (Arthur et al., 1985). The $\delta^{13}C_{org}$ values of Members 2 and 3 are more enriched (median = -28.7‰). However, this interval preserves high $\delta^{13}C_{org}$ variability (1σ SD±1.5‰). A sustained positive carbon isotope excursion (+3.0 to +4.5‰) is noted in Members 2 and 3 (1380-1440 m) corresponding closely to the timing of OAE3 as recorded by a +1‰ CIE in the WIB (Joo and Sageman, 2014). Smoothed $\Delta^{13}C$ in SK1-S decreases up-core from the base of Member 1 from ~36‰ to ~31‰, and further decreases by ~-3‰ through OAE3. In the Angus Core (WIB), smoothed $\Delta^{13}C$ records a similar but lower magnitude decrease (~-0.5‰) through OAE3. In that interval, $\delta^{13}C_{carb}$ is relatively stable (1σ SD±0.19‰) with average $\delta^{13}C_{carb}$ values (+1.84‰) comparable to coeval values in the English Chalk reference curve (Jarvis et al., 2006).

4.3 XRF data

Given that facies changes can significantly alter elemental chemistry of sediments, we limit discussion and interpretation of XRF data to the lacustrine facies of the Qingshankou Formation. Redox sensitive trace elements that accumulate in low oxygen conditions, such as Co, Cr, Ni, Pb, V, and Cu, show subtle to significant enrichment in the TOC-rich Qingshankou Member 1, whereas Mn, which remobilizes in anoxic environments, shows decreased concentrations (Table A.2). The V+Cr concentrations, a trace element proxy for nitrate reduction and low O_2 (Sageman et al., 2014a), are significantly enriched in Member 1 (>200 ppm) above background values for the Qingshankou Formation (~150 ppm) (Fig. 3). Copper concentrations spike at 1770 m and are strongly positively correlated with TOC ($r^2 = 0.87$) and C/N ($r^2 = 0.73$) in Member 1 (n=7).

Several trace elements and elemental ratios serve as proxies for water column euxinia where free hydrogen sulfide, a product of sulfate reduction, is present (Fig. 3) (Tribovillard et al., 2006). The V/(V+Ni) values, a proxy for anoxia and euxinia (Hatch and Leventhal, 1992), average 0.68-0.74 in the Qingshankou Formation with enrichments in Member 1 (0.74-0.77). Throughout the Qingshankou Formation the V/(V+Ni) ratios fall consistently into the non-sulfidic anoxic range. The concentrations of Mo, one of the most robust elemental indicators of euxinia, average 8 ppm (1σ SD±5 ppm, max [Mo] = 21.7 ppm) and show no notable increase in Qingshankou Member 1. Ratios of Mo/Al average $0.78x10^{-4}$ (1σ SD±$0.48x10^{-4}$) exceed average shale values ($0.32x10^{-4}$, Wedepohl, 1971) throughout most of the Qingshankou, suggesting authigenic enrichment. However, Mo/TOC is poorly correlated ($r^2 = 0.19$) and reaches a minimum in the TOC-rich Member 1. Despite high TOC, the S/Fe and Fe/Al ratios, which are known to increase with authigenic pyrite formation, do not increase in Member 1 (Fig.3). Also, we calculate the chemical index of alteration (CIA), which is a proxy for weathering intensity

(Table A.2; Fig. 3) (Nesbitt and Young, 1982). The carbonate corrected CIA is relatively stable throughout the Qingshankou Formation, although it does preserve a ~10% decrease during the OAE3 CIE, typically indicative of decreased weathering intensity.

4.4 Initial osmium isotope ratios

The Os_i from the Qingshankou Formation range between 0.66 and 0.96 (Figs. 2 & 6). Osmium concentrations are similar through the interval (^{192}Os conc. = 7-17 ppt; Table A.1). Rhenium concentrations are generally higher in Qingshankou Member 1 (avg. Re conc. = 3.80 ppb, 1σ SD±0.18 ppb) than in Members 2 and 3 (avg. Re conc. = 1.99 ppb, 1σ SD±1.66 ppb), except for one point at 1325 m (Table A.1). The Os_i values are the most radiogenic through the TOC-rich mudstones in the Member 1 (avg. Os_i = 0.90, 1σ SD±0.05) (Fig. 6). In the lowermost Members 2 and 3, one sample at ~1685 m yields a slightly less radiogenic value (Os_i = 0.76) compared to the samples below (Os_i = 0.87) and above (Os_i = 0.91). Relatively stable (Os_i range = 0.11) Os_i values from the upper sample set in Qingshankou Members 2 and 3 characterize the SK1-S interval spanning OAE3. The Os_i values in this interval are slightly less radiogenic (avg. Os_i = 0.72) than in Qingshankou Member 1.

A time correlative open marine section from ODP Site 1259 at Demerara Rise, yields samples highly enriched in osmium (^{192}Os conc. = 31-366 ppt) and highly variable in rhenium concentrations (Re conc. range = 12-142 ppb) (Table A.1.1). The Os_i values are more unradiogenic than values recorded in the Songliao Basin and are relatively stable over approximately 3 Ma, ranging between 0.55 and 0.71 (avg. Os_i = 0.61, 1σ SD±0.06) (Figs. 2 & 6; Table A.1.1). The Os_i samples from the marine WIB spanning OAE3 preserve no prominent excursion through the event (Os_i = 0.54-0.58) and are highly enriched in osmium (^{192}Os conc. = 136-260 ppt) and rhenium (Re conc. = 191-361 ppb).

5. Interpretation

5.1 Qingshankou Formation $\delta^{13}C_{org}$ chemostratigraphy and OAE3

Carbon isotope excursions have proven utility as isochronous horizons to correlate stratigraphic records globally (Jarvis et al., 2006; Wendler, 2013). However, a host of factors in a given sedimentary basin can alter bulk organic carbon isotopic ratios ($\delta^{13}C_{org}$) in addition to changes in the global carbon cycle, such as changing organic matter type and metabolic pathways. Our comparison of Gaussian kernel smoothed $\delta^{13}C_{org}$ records from the Songliao Basin and WIB (Joo and Sageman, 2014) demonstrates one negative CIE, possibly the Bridgewick Event (Jarvis et al., 2006), and one positive CIE, OAE3 (also referred to as the Whitefall/Kingsdown CIEs), which broadly correspond in age and duration (Fig. 4). Despite similar CIE durations, we detect an offset of 330 ka after cross-correlation of the two basins' anchored $\delta^{13}C_{org}$ time series, with ages of the Songliao Basin CIEs being older than ages of the WIB CIEs (see Fig. A.1). This offset could arise from the presence of "reworked and/or detrital zircon" in radioisotopically dated samples of SK1-S (Wang et al., 2016b), or undetected Upper Turonian/Lower Coniacian hiatuses in SK1-S or the WIB (Sageman et al., 2014b). Although partially offset in age, we note that these CIEs overlap within temporal uncertainty of time scales in the Songliao Basin (±181 ka, Sect. 3.1) and in the WIB (e.g., Turonian/Coniacian Boundary = ±380 ka; Sageman et al., 2014b). Moreover, the similarity in the timing and duration of CIEs signifies agreement between East Asian and North American time scales, validating intercontinental comparison of geologic datasets (e.g., paleoclimatic, paleobiologic). We note that the CIEs are amplified in the lacustrine Songliao Basin (+3.0 to +4.5‰) compared to the marine WIB (~+1‰) (Joo and Sageman, 2014) and other marine $\delta^{13}C_{carb}$ records in the WIB (Tessin et al., 2015; this study) and elsewhere (Wagreich, 2012; Wendler, 2013, and references therein).

The identification of OAE3 within a lake system in the terrestrial Qingshankou Members 2 and 3 permits comparisons to marine records of the event aided by a highly resolved temporal framework. The lowest TOC levels in the Qingshankou Formation in SK1-S occur during OAE3 (Fig. 2). This is also the case for OAE2, since the event is preserved in the TOC-lean Quantou Formation in SK1-S (Chamberlain et al., 2013). Accordingly, we confirm that OAEs do not necessarily correspond to lake anoxic events in East Asian lake systems (Wu et al., 2013), and that these lakes were not significant organic carbon depocenters during OAEs. We infer that during OAE3, reduced primary productivity and/or enhanced bottom-water oxygenation through regular lake overturning, in response to climatic forcing, played a role in decreasing organic carbon preservation.

In both SK1-S and the WIB, $\delta^{13}C_{org}$ enrichment and a diminutive excursion in $\delta^{13}C_{carb}$ (Fig. 2) (ostracod - Chamberlain et al., 2013) across OAE3 controls a decrease in $\Delta^{13}C$ (Fig. 5). In SK1-S, this $\delta^{13}C_{org}$ excursion is not likely due to changing organic matter source given consistently low C/N. Another coeval $\Delta^{13}C$ record from the Portland Core (Colorado) in the WIB with variable organic matter type has been interpreted as diagenetically altered (Tessin et al., 2015). However, there is little evidence for $\delta^{13}C_{org}$ or $\delta^{13}C_{carb}$ diagenesis in the Angus Core in the OAE3 interval (Appendix). Therefore, we attribute the OAE3 $\delta^{13}C_{org}$ excursion and decreased $\Delta^{13}C$ to diminished fractionation between dissolved inorganic carbon and photosynthate, driven by decreased dissolved CO_2 levels (Kump and Arthur, 1999). In the marine record, this is consistent with atmospheric pCO_2 drawdown commensurate with organic carbon sequestration in marine shales globally, as has been inferred for OAE2 (e.g., Jarvis et al., 2011).

291 However, lacustrine pCO_2 proxies (i.e., $\Delta^{13}C$) cannot be interpreted as direct records of
292 atmospheric pCO_2 since modern large lakes analogous to the depositional environment of the
293 Qingshankou Formation are net sources of CO_2 to the atmosphere, such as the East African rift
294 lakes (Alin and Johnson, 2007). Over longer time periods, riverine inputs of dissolved CO_2 are
295 the primary control on modern lacustrine CO_2 levels in mid-latitude lakes, and vary as a function
296 of soil pCO_2 and catchment productivity (Maberly et al., 2013). The sedimentary geochemistry
297 of modern and Lower Cretaceous rift lakes in Africa record these landscape processes as well
298 (Harris et al., 2004; Talbot et al., 2006), since dissolved CO_2 levels exert a significant control on
299 carbon isotope fractionation in lakes (Hollander and Smith, 2001). During OAE3, the Songliao
300 lake system preserves a comparatively larger shift in $\delta^{13}C_{org}$ and $\Delta^{13}C$ than the WIB (Fig. 5). We
301 attribute this to a greater decrease in dissolved CO_2 in the Songliao lake system, driven by
302 reduced soil productivity in the basin's catchment through OAE3. This is consistent with a
303 scenario of atmospheric pCO_2 drawdown and cooling reflected in decreased marine $\Delta^{13}C$ in the
304 WIB.

305 Compared to OAE2, pCO_2 drawdown through OAE3 is interesting since the event is not
306 represented by a discrete archetypal black shale or anoxic/euxinic interval (Wagreich, 2012;
307 Lowery et al., 2017) and preserves a relatively diminished marine CIE (Jarvis et al., 2006;
308 Locklair et al., 2011; Joo and Sageman, 2014). One mechanism for sustaining an OAE invokes
309 enhanced weathering of continentally derived nutrients (e.g., P), following volcanic CO_2 pulses
310 from large igneous province (LIPs) emplacement (cf. Jenkyns, 2010). However, marine Os_i
311 values spanning OAE3 in the WIB do not record evidence for submarine LIP volcanism (i.e.,
312 unradiogenic Os_i shift) (Fig. 6; Sect. 5.3), as is the case for OAE2 (Turgeon and Creaser, 2008;
313 Du Vivier et al., 2014); nor do they record evidence for accelerated global continental

weathering rates (i.e., a shift to more radiogenic Os_i). Likewise, weathering proxies from the Songliao Basin's OAE3 interval are either stable, such as Os_i (Figs. 2 & 6), or suggest a decrease in weathering intensity, such as $\Delta^{13}C$ (Fig. 4) and CIA (Fig. 3). Although we caution that these local observations are of a relatively minor OAE and cannot be assumed globally representative, these results suggest that the perturbations to the Earth system that triggered and sustained OAE3 are unique from those that triggered more severe OAEs (e.g., OAE2, Toarcian OAE).

Overall, the Qingshankou Formation $\delta^{13}C_{org}$ chemostratigraphy is highly variable through Member 1 and the lowermost Members 2 and 3. This suggests that dynamic local biogeochemical cycling and environmental conditions, in addition to the global carbon cycle, affected the $\delta^{13}C_{org}$ values in this interval (Fig. 2). Furthermore, we interpret the combination of highly depleted $\delta^{13}C_{org}$ values (-32.4‰ minimum), high C/N typical of nitrogen-poor anoxic bottom-waters (Meyers, 1994), and redox-sensitive XRF data (Sect 5.2), as evidence that methanogenesis and methanotrophy (Hollander and Smith, 2001) influenced bulk $\delta^{13}C_{org}$ values in the TOC-rich Qingshankou Member 1. Extremely $\delta^{13}C$ depleted methyl hopane compounds (-42 to -50‰) in Member 1 equivalent oil shales from the Ngn-02 Core (Bechtel et al., 2012) confirm the role of methanotrophy in the unit. As a result, we cannot solely attribute the depleted $\delta^{13}C_{org}$ in Member 1 to the global Bridgewick CIE, and instead we interpret this interval as at least partially recording burial of lacustrine methanotrophic biomass. Increased dissolved CO_2 in the lake from increased catchment productivity may have also contributed to the amplified negative CIE in Member 1 (Hu et al., 2015).

5.2 Low sulfate and redox conditions in lacustrine Qingshankou Formation

The redox sensitive trace element dataset from Qingshankou Member 1 (Sect. 4.3) provides a record of non-euxinic anoxic bottom-waters during deposition. Consistent trends among a

variety of the evaluated trace element proxies lend confidence to the paleo-redox reconstructions. Combined, low Mn (<400 ppm), elevated V+Cr (>200 ppm) and (V+Cr)/Al, and elevated V/(V+Ni) (>0.7, Hatch and Leventhal, 1992) in Member 1 indicate anoxia (Fig. 3).

Compared to the marine realm, biogeochemical cycling in anoxic lakes typically operates with fundamentally different dominant microbial pathways (e.g., methanogenesis and methanotrophy), since lakes generally have much lower concentrations of dissolved sulfate and redox-sensitive trace elements such as molybdenum. Microbial sulfate reduction (MSR) in anoxic low sulfate lakes tends to draw down the sulfate reservoir and limit sulfur isotope fractionation leaving pyrite isotopic values enriched (Gomes and Hurtgen, 2013). In Qingshankou Member 1, $\delta^{34}S_{pyrite}$ is highly enriched (+15 to +20‰) (Fig. 3) (Huang et al., 2013). Huang et al. (2013) attributed this to a complex disproportionation and transport model dependent on isotopic heterogeneity within the basin. However, considering our new trace element data, we propose an alternative interpretation, namely that the enriched $\delta^{34}S_{pyr}$ values were consequences of inhibited MSR fractionation related to low sulfate concentrations under non-marine depositional conditions. This phenomenon is noted in Holocene non-marine Black Sea mudstones (>~8 ka) deposited during basin isolation from the global ocean (Calvert et al., 1996). In another test of sulfate levels and seawater connectivity, TOC/S ratios are generally <2.8 in marine sediments (Berner, 1982), although some lacustrine mudstone values fall below this threshold (e.g., Calvert et al., 1996). In Qingshankou Member 1, TOC/S ratios all exceed this threshold (average TOC/S = 14; this study) and are consistent with pyrite burial limited by low sulfate levels (Bechtel et al., 2012). Concentrations of molybdenum (average = 8 ppm), another robust proxy for the presence of free sulfide, remain below minimum thresholds established for euxinic mudstones (25 ppm Mo-depleted waters, 65 ppm Mo-replete waters,

Scott and Lyons, 2012), but molybdenum concentrations and Mo/Al values do exceed average shale values (2.6 ppm and $0.32x10^{-4}$ respectively, Wedepohl, 1971), suggesting MSR was active, but limited by low sulfate and molybdate concentrations in the lake (Fig. 3). In Mo-replete marine waters, sedimentary Mo concentrations positively correlate with TOC (Algeo and Lyons, 2006). However, this relationship is not observed in the Qingshankou Formation ($r^2 = 0.19$) and Mo/TOC ratios are lowest in the TOC-rich Member 1 (Fig. 3) (Sect. 4.3). Influxes of sulfate and molybdenum-replete marine water would have elevated MSR and corresponding pyrite burial, leading to increases in Fe/Al, Mo/TOC, and S concentrations. Our proxy results from SK1-S do not record such shifts, and we therefore infer that low sulfate non-marine conditions prevailed throughout deposition of the Qingshankou Formation.

Depleted bulk $\delta^{13}C_{org}$ (*this study*; Hu et al., 2015) and methyl hopane $\delta^{13}C$ values (Bechtel et al., 2012) reinforce the hypothesis that sulfate reduction was limited and that methanogenic and methanotrophic microbial metabolisms were prevalent during deposition of Qingshankou Member 1 (Sect. 5.1). Additionally, concentrations of certain trace elements, such as Cu, Ni, Co, that play central roles in enzymes facilitating methanogenesis and methanotrophy (Glass and Orphan, 2012), spike in Member 1. This may indicate enhanced methanogenesis and methanotrophy in the anoxic lacustrine mudstones (Fig. 3). Alternatively, it could reflect that metals are complexed with organic matter independent of methantrophic activity in Member 1 (TOC and Cu covariance: $r^2 = 0.88$). Regardless, proxies such as elemental concentrations, methanotrophic biomarkers, sulfur isotopes, laminated mudstones, and bulk $\delta^{13}C_{org}$, consistently indicate persistent anoxia and methanogenesis in low sulfate waters (i.e., MSR inhibited) during deposition of the TOC-rich Qingshankou Member 1.

5.3 Seawater incursion hypothesis and Os_i chemostratigraphy

383 Incursions of dense marine water into the Songliao Basin during sea level highstands
384 have been invoked as a mechanism to stratify the basin's water column, intensifying bottom-
385 water anoxia, and ultimately driving deposition of Member 1's TOC-rich source rocks (Hou et
386 al., 2000; Huang et al., 2013; Hu et al., 2015). Mixing of marine and lacustrine water bodies,
387 each with distinct chemical properties, would perturb the chemostratigraphic record, including
388 Os_i values. However, our Os_i chemostratigraphy from SK1-S preserves no compelling evidence
389 for marine incursions in TOC-rich intervals. Instead, the Os_i data in Member 1 are consistently
390 the most radiogenic values of SK1-S (Fig. 6). We conclude that this observation is inconsistent
391 with incursions of less radiogenic open marine osmium as measured at Demerara Rise, and
392 resembles the more radiogenic Os_i records existing from lacustrine mudstones elsewhere (Poirier
393 and Hillaire-Marcel, 2011; Cumming et al., 2012; Xu et al., 2017). At Demerara Rise, an
394 average open marine Os_i of ~0.6 for mid-Turonian to Coniacian samples is considered to be the
395 best estimate of the steady-state open marine value for the Late Cretaceous governed by plate
396 tectonic configurations (i.e., long-term average continental weathering and hydrothermal fluxes)
397 given similar results from comparably aged marine records, such as post-OAE2 (Du Vivier et al.,
398 2014) and our new WIB OAE3 data (Fig. 6). However, we note that the WIB Os_i data is likely
399 more radiogenic than open marine Os_i, due to the marine basin's epicontinental setting and
400 mixing with continentally derived osmium.

401 One Os_i data point (1685 m) in the lower Songliao Os_i sample set is less radiogenic than
402 other nearby horizons. This is also an interval where concentrations of 24-n-
403 isopropylchlorestane spike (biomarker typically attributed to marine organisms, Hu et al., 2015)
404 and XRF sulfur concentrations more than double for one data point. It is possible that this
405 horizon indicates a minor seawater incursion. However, we consider that this is unlikely since

406 the horizon is not associated with any spikes in euxinic-sensitive trace elements (e.g., Mo,
407 V/V+Ni, Sect. 5.2) (Fig. 3), TOC enrichments, or changes in lithology, and due to additional
408 paleogeographic factors discussed below.

409 Our trace element and Os_i evidence contrary to a Songliao Basin-marine connection
410 during deposition of Qingshankou Member 1 is consistent with many lines of previous
411 observation such as: a lack of foraminifera, calcareous nannofossil, or marine macrofossil
412 preservation in the Qingshankou Formation of SK1-S (Wan et al., 2013; Xi et al., 2016), non-
413 marine phytoplankton (Zhao et al., 2014), depleted non-marine $\delta^{18}O$ values (Chamberlain et al.,
414 2013), plate tectonic reconstructions placing the nearest marine body at least 500 km away, and
415 evidence for coastal mountain building between the Songliao Basin and Pacific Ocean (Yang,
416 2013) (Fig.1). Contrastingly, observations of $\delta^{34}S_{pyr}$ (Huang et al., 2013) and biomarkers (C30
417 steranes e.g., 24-isopropylchlorestane, Hu et al., 2015) have been interpreted as evidence for
418 marine incursions. Additionally, a few poorly preserved foraminifera have been reported in
419 Member 1 elsewhere in the basin (Xi et al., 2016), although no photographs or depths of
420 occurrence are accessible to our knowledge, precluding verification, taxonomic identification,
421 and correlation to horizons in the SK1-S core. It is possible to reconcile our geochemical
422 datasets with enriched $\delta^{34}S_{pyr}$ data in Member 1 if a low sulfate lake water column inhibited
423 sulfur isotope fractionation (Sect. 5.2). Explaining the presence of 24-n-isopropylchlorestane
424 without invoking seawater incursions is more challenging, because the biomarker has been
425 classified as an indicator of marine organic matter (Moldowan et al., 1990). However, we note
426 that C30 steranes, including molecular precursors to 24-isopropylcholestane, have been detected
427 in a modern French lake (Wunsche et al., 1987). If the biomarkers previously reported from the
428 Songliao Basin (Hu et al., 2015) are instead derived from non-marine dinoflagellates, sponges or

429 microbial symbionts producing C30 sterols, are detritally re-worked, or are the molecular
430 diagenetic products of organic matter degradation in a thermally mature interval of the basin (cf.
431 Feng et al., 2010), then their occurrences would be consistent with our interpretation of the Os_i
432 record as that of an isolated lacustrine basin.

433 Alternatively, our Os_i record from the Songliao Basin could have been dominated by a
434 high flux of continentally derived radiogenic Os_i from nearby catchments, masking a record of
435 seawater incursions via mixing. A recent study of Holocene Os_i profiles in a transect off
436 Greenland's coast demonstrated that Os_i records can be sensitive to local fluxes of weathered
437 osmium (Rooney et al., 2016). However, we consider that this masking scenario is less likely in
438 the Songliao Basin, since Members 2 and 3 lack evidence for marine incursions, but do not show
439 evidence for extremely radiogenic Os_i values within the weathered catchments (Fig. 6).
440 Additionally, two strontium isotope measurements in the lower Qingshankou Formation (avg.
441 $^{87}Sr/^{86}Sr = 0.70767$, 1σ SD±0.00005) are not extremely radiogenic, but are offset from coeval
442 marine ratios (Chamberlain et al., 2013). Their values do not preserve evidence for marine
443 incursions, nor do they indicate weathering of extremely radiogenic lithologies within the basin's
444 catchment. This suggests that Os_i chemostratigraphy could resolve evidence of marine
445 incursions if present. We note that it is possible that a brief marine incursion occurred in an
446 unsampled interval, as temporal resolution of Os_i samples range from 100-300 ka in Member 1.
447 However, we selected samples from horizons with published proposed evidence (i.e., biomarker)
448 for marine incursions (Fig. 6). Additionally, we observe no abrupt lithologic alterations in SK1-
449 S commonly associated with lacustrine-marine transitions in other basins (Calvert et al., 1996;
450 Poirier and Hillaire-Marcel, 2011 and references therein).

In the younger OAE3 interval of Qingshankou Members 2 and 3, the Os_i data are less radiogenic, and approach values from the epicontinental marine WIB (Fig. 6). Again, we do not interpret these data as evidence for a prolonged marine connection to the Songliao Basin, because little evidence exists of marine microfossils (Xi et al., 2016) or sulfate replete waters (Sect. 5.2; Fig. 3) in this interval. Instead, we attribute the lower Os_i values in Qingshankou Members 2 and 3 to the weathering of the near contemporaneous mid-Coniacian flood basalts within the Songliao Basin (Wang et al., 2016a), which would possess mantle-like $^{187}Os/^{188}Os$ compositions (~0.13) mixing with lake waters (Fig. 6). We also note that Os_i values are relatively stable through OAE3, suggesting muted changes in the weathering flux of osmium (Sect. 5.1).

5.4 Qingshankou Formation Depositional Model

Given limited evidence for incursions of saline marine waters in Member 1 (Sect. 5.2-5.3), we propose alternative mechanisms for lake stratification that could be responsible for enhanced anoxia (Sect. 5.1-5.2) and resulting enhanced organic matter burial. Based on modern and paleo analogs, we outline a new conceptual model characterizing bottom-water redox, biogeochemical cycling, and physical processes (stratification, mixing) for the lacustrine Songliao rift basin through the Qingshankou Formation interval (Fig. 7). Sustained stratification of large meromictic lakes is critical in generating TOC-rich mudstone deposits, as settling organic matter from highly productive lacustrine surface waters is remineralized passing through isolated and progressively deoxygenated bottom-waters (Demaison and Moore, 1980). For any scenario of bottom-water anoxia, the depth of the stratified lake would need to exceed the wave-base mixing depth. This considerable minimum depth (e.g., ~100 m) on a large paleolake with an expansive fetch (~200-300 km) for generating waves, supports the assertion that the lake was

474 deeper and more expansive during Member 1 than Members 2-3 (Feng et al., 2010), favoring
475 meromixis within a deep lake.

476 Water column density stratification likely arose in Qingshankou Member 1 from
477 gradients in temperature, salinity, temperature, and/or dissolved gases from organic matter
478 remineralization (e.g., Boehrer and Schultze, 2008), inhibiting lake overturning and
479 reoxygenation of bottom-waters (Fig. 7). In the case of thermal stratification, most modern
480 meromictic lakes do not occur outside the tropics (e.g., Lake Tanganyika), and are reinforced by
481 additional density gradients. However, the mid-Cretaceous was a period of extreme greenhouse
482 warmth. Intervals of high temperature and low seasonality (i.e., obliquity minima) would have
483 inhibited the Songliao Basin water column overturning and reduced dissolved oxygen levels, and
484 indeed palynological datasets indicate a semi-humid subtropical climate during deposition of
485 Member 1 (Wang et al., 2013; Zhao et al., 2014). Although additional paleoclimate data are
486 necessary to fully test this hypothesis, our idea that elevated temperatures would have inhibited
487 lake overturning is consistent with general reconstructions for the warm mid-Cretaceous. Even
488 though we do not detect seawater incursions in this study and no evaporites are associated with
489 Member 1, evidence for elevated salinity is inferred from paleontological investigations that
490 have documented slightly brackish algae, dinoflagellate, and ostracod assemblages (Zhao et al.,
491 2014; Xi et al., 2016). Organic geochemical investigations have also detected salinity biomarkers
492 (e.g., gammacerane, β-carotane) in Member 1 (Bechtel et al., 2012). Several ostracod $\delta^{18}O$ and
493 $\delta^{13}C_{carb}$ values are enriched in Member 1 and lowermost Members 2 and 3 compared to
494 overlying samples (Chamberlain et al., 2013), possibly related to enhanced evaporation rates and
495 consistent with dolomite laminae preservation in the interval (Talbot, 1990; Gao et al., 2009;
496 Wang et al., 2009). Further, authors interpret covariation between $\delta^{18}O$, $\delta^{13}C_{carb}$, Mg/Ca, and

Sr/Ca as evidence for closed basin conditions throughout the Qingshankou Formation, signifying a lake basin sensitive to changing precipitation to evaporation (P/E) rates (Chamberlain et al., 2013). On the other hand, palynology suggests the climate was semi-humid during Member 1 (Wang et al., 2013) which would have limited evaporation and salinity's role in density stratification, although others report that diagenesis possibly biased palynological reconstructions (Zhao et al., 2014). A final process that we suspect contributed to elevated bottom-water density in Lake Songliao is the addition of dissolved biochemical products (e.g., HCO_3^-, H_2S, CH_4, etc.) from remineralization of organic matter (Fig. 7a). Evidence for methanogenesis, as well as heterotrophic biomarkers (e.g., hopanoids) (Bechtel et al., 2012), indicate microbial reworking of biomass in Member 1. This is consistent with increased bottom-water density via "biogenic meromixis", stratification from dissolved biochemical products (Boehrer and Schultze, 2008). Our combined model for Lake Songliao's stratification draws on many physical and geochemical processes, such as temperature gradients, biogenic meromixis, and elevated salinity. We hypothesize that these processes were controlled both by tectonic (i.e., lake depth) and climatic (e.g., P/E) conditions that contributed to a stagnant pool of anoxic bottom-water conducive to deposition of TOC-rich mudstones.

Conversely in Members 2 and 3, we propose that TOC-lean grey mudstones were the result of enhanced water column overturning and improved oxygenation of lake bottom-waters. During OAE3, the interval of lowest TOC in the Qingshankou Formation, factors such as, increased seasonality, freshening of bottom-waters, more vigorous wave mixing (i.e., higher surface wind velocity), and/or lake shallowing likely contributed to bottom-water reoxygenation and the demise of stratification (Fig. 7b).

6. Conclusions

Through geochemical analyses, we reconstruct local Late Cretaceous paleoclimate records and lacustrine carbon burial dynamics of the Qingshankou Formation in the Songliao Basin of northeast China. Correlation of Turonian-Coniacian $\delta^{13}C_{org}$ records from the Songliao Basin to the WIB confirms the presence of OAE3 in a low-TOC interval of Qingshankou Members 2 and 3, providing a unique record OAE3 in a lake system. The chemostratigraphic results from the Songliao Basin demonstrate that OAE2 and OAE3 did not trigger elevated organic carbon burial in an expansive East Asian lake. Furthermore, we attribute significant decreases in marine and lacustrine $\Delta^{13}C$ to a drawdown of pCO_2 and cooling through OAE3 and decreased soil productivity in the Songliao catchment. This finding is consistent with enhanced burial of organic carbon on a global scale and is analogous to interpretations for other prominent Cretaceous OAEs (Arthur et al., 1988; Barclay et al., 2010; Jarvis et al., 2011). However, Os_i stratigraphy records no evidence for significant changes in global volcanism though OAE3, which suggests an event trigger unique from OAE2 (i.e., LIP volcanism). We encourage future investigations, employing, for example, compound specific $\delta^{13}C$ chemostratigraphy and high-resolution paleoclimate proxies, to further resolve the robustness of $\delta^{13}C$ correlations and better elucidate the paleoclimatic response of the Songliao basin lacustrine units to OAE3.

Radiogenic Os_i values recorded through the TOC-rich Qingshankou Member 1 indicate that enhanced organic carbon burial and source rock formation occurred in a lacustrine basin isolated from the global ocean. Although our Os_i sample resolution is limited and marine incursions could have alluded detection in this initial survey, our higher resolution redox sensitive trace element data, as well as most existing paleogeographic, chemostratigraphic, and paleobiologic data, are also consistent with mudstone deposition in a low sulfate, lacustrine setting through Member 1. Our synthesis of existing stratigraphic datasets into a source rock depositional model

543 for Qingshankou Member 1 outlines lacustrine stratification and biogeochemical cycling
544 scenarios independent of marine incursions. This study underscores the potential to reconstruct
545 Late Cretaceous paleoclimate, lake system responses to OAEs, and terrestrial carbon burial
546 dynamics from lacustrine mudstones archives, such as those found in the Songliao Basin.

Acknowledgements

We thank Professor Chengshan Wang (China University of Geosciences, Beijing) for facilitating sampling of the SK1-S core. This research also benefited greatly from the assistance of Northwestern University lab managers Grace Schellinger and Dr. Koushik Dutta, and research assistant Katarina Savatic during measurement of carbon chemistry; Antonia Hofmann and Dr. Joanna Hesselink of Durham University with rhenium-osmium isotope analyses; and Juan Lezama-Pacheco and Danielle Moragne at Stanford University with XRF analyses. We thank three anonymous reviewers who provided valuable feedback and improved the quality of the manuscript. U.S. National Science Foundation grant funding was provided to B.B.S. (EAR-1424474), and to C.P.C. and S.A.G. (EAR-1423967). National Basic Research Program of China funding was provided to Y.G. (2012CB8220000). D.S. acknowledges the TOTAL Endowment Fund.

Appendix A. Supplementary material

Supplementary material for this article can be found online at (link)

563 **Figure Captions**

564 **Fig. 1: a.)** Palinspastic map of East Asia during the Coniacian-E. Campanian, including the
565 studied Songliao Basin and surrounding physical geographic and plate tectonic features
566 (SYB=Subei-Yellow Sea Basin; modified from Yang, 2013). **b.)** Map of SK1-S core and facies
567 during deposition of Qingshankou Member 1 (modified from Feng et al., 2010). **c.)** Cross section
568 A-A' from Wang et al. (2013) depicting Cretaceous lithostratigraphic units of the Songliao Basin
569 including the Qingshankou Formation (dark blue).

570 **Fig. 2:** Chemostratigraphic record from SK1-S core spanning the upper Quantou through the
571 Yaojia formations. Stratigraphic column modified from Wu et al. (2013). Red stars represent
572 bentonite horizons with CA-ID-TIMS U/Pb zircon ages (Wang et al., 2016). Hiatus at the
573 Qingshankou/Yaojia contact identified by Feng et al. (2010). The $\delta^{13}C_{carb}$ (red) data are from
574 Chamberlain et al. (2013) and faded gray $\delta^{13}C_{org}$ values from Hu et al. (2015).

575 **Fig. 3:** Trace element concentration data from Qingshankou Member 1 and Qingshankou
576 Members 2 and 3 in the SK1-S core. Detrital proxies include the chemical index of alteration
577 (CIA). Redox thresholds for V/V+Ni are from Hatch and Leventhal (1992). Dashed lines in Mn
578 and V+Cr plots represent median concentrations. $\delta^{34}S_{pyr}$ data are from Huang et al. (2013).
579 Redox thresholds for Mo concentrations from Scott & Lyons (2012).

580 **Fig. 4:** Correlation of $\delta^{13}C_{org}$ time series from the Songliao Basin (*this study*) and Western
581 Interior Basin (N. America) (Joo & Sageman, 2014). Red lines represent Gaussian kernel
582 smoothed $\delta^{13}C_{org}$ values ($\sigma = \pm 150$ ka). The Songliao time scale derived from astronomical time
583 scale (Wu et al., 2013) anchored to a U/Pb zircon age date (Wang et al., 2016) (Sect. 3.1 and
584 appendix).

585 **Fig. 5:** Record of $\Delta^{13}C$ ($\delta^{13}C_{carb}$ - $\delta^{13}C_{org}$) changes, approximating carbon isotope fractionation
586 across OAE3 in the Songliao Basin and Western Interior Basin (WIB) of North America. Red
587 lines represent Gaussian kernel smoothed $\Delta^{13}C$ values ($\sigma = \pm 150$ ka).

588 **Fig. 6:** Comparison of Os_i time series from the Songliao Basin SK1-S (green) and Demerara
589 Rise ODP Site 1259 (blue). Time scales from Songliao Basin (Wu et al., 2013; Wang et al.
590 2016), Demerara Rise (updated from Bornemann et al., 2008), and WIB (Joo and Sageman,
591 2014). Flood basalt emplacement in black (Wang et al., 2016a). Previously cited evidence for
592 the Qingshankou Formation marine incursions in yellow shaded intervals for presence of marine
593 biomarkers (Hu et al., 2015) and purple interval of $\delta^{34}S_{pyr}$ data (Huang et al., 2013).

594 **Fig. 7: a.)** Non-marine biogeochemical and depositional model of Qingshankou Member 1 also
595 depicting theoretical plots of density (ρ), salinity, total dissolved substances (TDS), and winter
596 and summer water temperature profiles. **b.)** Biogeochemical cycling and depositional model for
597 Qingshankou Members 2 and 3 during OAE3 interval. See text for discussion.

References

Algeo, T. J., Lyons, T. W., 2006. Mo–total organic carbon covariation in modern anoxic marine environments: Implications for analysis of paleoredox and paleohydrographic conditions: Paleoceanography. 21, 1

Alin, S.R., Johnson, T.C., 2007. Carbon cycling in large lakes of the world: A synthesis of production, burial, and lake-atmosphere exchange estimates. Global Biogeochem. Cycles. 21

Arthur, M.A., Dean, W.E., Claypool, G.E., 1985. Anomalous C-13 enrichment in modern marine organic-carbon. Nature 315, 216-218.

Arthur, M.A., Dean, W.E., Pratt, L.M., 1988. Geochemical and climatic effects of increased marine organic-carbon burial at the Cenomanian-Turonian Boundary. Nature 335, 714-717.

Barclay, R.S., McElwain, J.C., Sageman, B.B., 2010. Carbon sequestration activated by a volcanic CO2 pulse during Ocean Anoxic Event 2. Nat Geosci 3, 205-208.

Bechtel, A., Jia, J.L., Strobl, S.A.I., Sachsenhofer, R.F., Liu, Z.J., Gratzer, R., Puttmann, W., 2012. Palaeoenvironmental conditions during deposition of the Upper Cretaceous oil shale sequences in the Songliao Basin (NE China): Implications from geochemical analysis. Organic Geochemistry 46, 76-95.

Berner, R.A., 1982. Burial of organic-carbon andy pyrite sulfur in the modern ocean – its geochemical and environmental significance. American Journal of Science 282, 451-473.

Boehrer, B., Schultze, M., 2008. Stratification of lakes. Rev. Geophys. 46, 27.

Bornemann, A., Norris, R.D., Friedrich, O., Beckmann, B., Schouten, S., Damste, J.S.S., Vogel, J., Hofmann, P., Wagner, T., 2008. Isotopic evidence for glaciation during the Cretaceous supergreenhouse. Science 319, 189-192.

Calvert, S.E., Thode, H.G., Yeung, D., Karlin, R.E., 1996. A stable isotope study of pyrite formation in the Late Pleistocene and Holocene sediments of the Black Sea. Geochim Cosmochim Ac 60, 1261-1270.

Chamberlain, C.P., Wan, X., Graham, S.A., Carroll, A.R., Doebbert, A.C., Sageman, B.B., Blisniuk, P., Kent-Corson, M.L., Wang, Z., Wang, C., 2013. Stable isotopic evidence for climate and basin evolution of the Late Cretaceous Songliao basin, China. Palaeogeography Palaeoclimatology Palaeoecology 385, 106-124.

Cumming, V.M., Selby, D., Lillis, P.G., 2012. Re-Os geochronology of the lacustrine Green River Formation: Insights into direct depositional dating of lacustrine successions, Re-Os systematics and paleocontinental weathering. Earth Planet Sc Lett 359, 194-205.

Demaison, G., Moore, G.T., 1980. Anoxic environments and oil source bed genesis. Organic Geochemistry 2, 9-31.

Du Vivier, A.D.C., Selby, D., Sageman, B.B., Jarvis, I., Groecke, D.R., Voigt, S., 2014. Marine Os-187/Os-188 isotope stratigraphy reveals the interaction of volcanism and ocean circulation during Oceanic Anoxic Event 2. Earth Planet Sc Lett 389, 23-33.

Feng, Z.-q., Jia, C.-z., Xie, X.-n., Zhang, S., Feng, Z.-h., Cross, T.A., 2010. Tectonostratigraphic units and stratigraphic sequences of the nonmarine Songliao basin, northeast China. Basin Research 22, 79-95.

Gannoun, A., Burton, K.W., 2014. High precision osmium elemental and isotope measurements of North Atlantic seawater. Journal of Analytical Atomic Spectrometry 29, 2330-2342.

Gao, Y., Wang, P., Cheng, R., Wang, G., Wan, X., Wu, H., Wang, S., Liang, W., 2009. Description of Cretaceous Sedimentary Sequence of the First Member of the Qingshankou Formation Recovered by CCSD-SK-Is Borehole in Songliao Basin: Lithostratigraphy, Sedimentary Facies, and Cyclic Stratigraphy. Earth Science Frontiers 16, 314-323.

644 Glass, J.B., Orphan, V.J., 2012. Trace Metal Requirements for Microbial Enzymes Involved in the
645 Production and Consumption of Methane and Nitrous Oxide. Frontiers in Microbiology 3, 61.
646 Gomes, M.L., Hurtgen, M.T., 2013. Sulfur isotope systematics of a euxinic, low-sulfate lake: Evaluating
647 the importance of the reservoir effect in modern and ancient oceans. Geology 41, 663-666.
648 Graham, S.A., Hendrix, M.S., Johnson, C.L., Badamgarav, D., Badarch, G., Amory, J., Porter, M., Barsbold,
649 R., Webb, L.E., Hacker, B.R., 2001. Sedimentary record and tectonic implications of Mesozoic
650 rifting in southeast Mongolia. Geological Society of America Bulletin 113, 1560-1579.
651 Hatch, J.R., Leventhal, J.S., 1992. Relationship between inferred redox potential of the depositional
652 environment and geochemistry of the Upper Pennsylvanian (Missourian) Stark Shale Member of
653 the Dennis Limestone, Wabaunsee County, Kansas, U.S.A. Chemical Geology 99, 65-82.
654 Harris, N.B., Freeman, K.H., Pancost, R.D., White, T.S., and Mitchell, G.D., 2004. The character and origin
655 of lacustrine source rocks in the Lower Cretaceous synrift section, Congo Basin, west Africa.
656 AAPG Bulletin 88(8), 1163-1184
657 Hollander, D.J., Smith, M.A., 2001. Microbially mediated carbon cycling as a control on the delta C-13 of
658 sedimentary carbon in eutrophic Lake Mendota (USA): New models for interpreting isotopic
659 excursions in the sedimentary record. Geochim Cosmochim Ac 65, 4321-4337.
660 Hou, D., Li, M., Huang, Q., 2000. Marine transgressional events in the gigantic freshwater lake Songliao:
661 paleontological and geochemical evidence. Organic Geochemistry 31, 763-768.
662 Hu, J.F., Peng, P.A., Liu, M.Y., Xi, D.P., Song, J.Z., Wan, X.Q., Wang, C.S., 2015. Seawater Incursion Events
663 in a Cretaceous Paleo-lake Revealed by Specific Marine Biological Markers. Scientific Reports 5,
664 9508.
665 Huang, Y.J., Yang, G.S., Gu, J., Wang, P.K., Huang, Q.H., Feng, Z.H., Feng, L.J., 2013. Marine incursion
666 events in the Late Cretaceous Songliao Basin: Constraints from sulfur geochemistry records.
667 Palaeogeography Palaeoclimatology Palaeoecology 385, 152-161.
668 Jarvis, I., Gale, A.S., Jenkyns, H.C., Pearce, M.A., 2006. Secular variation in Late Cretaceous carbon
669 isotopes: a new delta C-13 carbonate reference curve for the Cenomanian-Campanian (99.6-
670 70.6 Ma). Geological Magazine 143, 561-608.
671 Jarvis, I., Lignum, J.S., Groecke, D.R., Jenkyns, H.C., Pearce, M.A., 2011. Black shale deposition,
672 atmospheric CO2 drawdown, and cooling during the Cenomanian-Turonian Oceanic Anoxic
673 Event. Paleoceanography 26.
674 Jenkyns, H.C., 2010. Geochemistry of oceanic anoxic events. Geochemistry Geophysics Geosystems 11.
675 Joo, Y.J., Sageman, B.B., 2014. Cenomanian to Campanian carbon isotope chemostratigraphy from the
676 Western Interior Basin, USA. Journal of Sedimentary Research 84, 529-542.
677 Kump, L.R., Arthur, M.A., 1999. Interpreting carbon-isotope excursions: carbonates and organic matter.
678 Chemical Geology 161, 181-198.
679 Kuroda, J., Jiménez-Espejo, F.J., Nozaki, T., Gennari, R., Lugli, S., Manzi, V., Roveri, M., Flecker, R., Sierro,
680 F.J., Yoshimura, T., Suzuki, K., Ohkouchi, N., 2016. Miocene to Pleistocene osmium isotopic
681 records of the Mediterranean sediments. Paleoceanography 31, 148-166.
682 Locklair, R., Sageman, B., Lerman, A., 2011. Marine carbon burial flux and the carbon isotope record of
683 Late Cretaceous (Coniacian-Santonian) Oceanic Anoxic Event III. Sedimentary Geology 235, 38-
684 49.
685 Locklair, R.E., Sageman, B.B., 2008. Cyclostratigraphy of the Upper Cretaceous Niobrara Formation,
686 Western Interior, USA: A Coniacian-Santonian orbital timescale. Earth Planet Sc Lett 269, 539-
687 552.
688 Ludvigson, G.A., Joeckel, R.M., González, L.A., Gulbranson, E.L., Rasbury, E.T., Hunt, G.J., Kirkland, J.I.,
689 Madsen, S., 2010. Correlation of Aptian-Albian Carbon Isotope Excursions in Continental Strata
690 of the Cretaceous Foreland Basin, Eastern Utah, U.S.A. Journal of Sedimentary Research 80, 955.

691 Lowery, C.M., Leckie, R.M., Sageman, B.B., 2017. Micropaleontological evidence for redox changes in the
692 OAE3 interval of the US Western Interior: Global vs. local processes. Cretaceous Research 69,
693 34-48.
694 Maberly, S.C., Barker, P.A., Stott, A.W., De Ville, M.M., 2013. Catchment productivity controls CO_2
695 emissions from lakes. Nat. Clim. Chang. 3, 391-394.
696 MacLeod, K.G., Huber, B.T., Jimenez Berrocoso, A., Wendler, I., 2013. A stable and hot Turonian without
697 glacial delta O-18 excursions is indicated by exquisitely preserved Tanzanian foraminifera.
698 Geology 41, 1083-1086.
699 Meyers, P.A., 1994. Preservation of elemental and isotopic source identification of sedimentary organic-
700 matter. Chemical Geology 114, 289-302.
701 Moldowan, J.M., Fago, F.J., Lee, C.Y., Jacobson, S.R., Watt, D.S., Slougui, N.-E., Jeganathan, A., Young,
702 D.C., 1990. Sedimentary 24-n-Propylcholestanes, Molecular Fossils Diagnostic of Marine Algae.
703 Science 247, 309-312.
704 Nesbitt, H.W., Young, G.M., 1982. Early Proterozoic climates and plate motions inferred from major
705 element chemistry of lutites. Nature 299, 715-717.
706 Oxburgh, R., 2001. Residence time of osmium in the oceans. Geochemistry, Geophysics, Geosystems 2.
707 Pagani, M., Huber, M., Sageman, B., 2014. 6.13 - Greenhouse Climates A2 - Holland, Heinrich D, in:
708 Turekian, K.K. (Ed.), Treatise on Geochemistry (Second Edition). Elsevier, Oxford, pp. 281-304.
709 Peucker-Ehrenbrink, B., Ravizza, G., 2000. The marine osmium isotope record. Terra Nova 12, 205-219.
710 Poirier, A., Hillaire-Marcel, C., 2011. Improved Os-isotope stratigraphy of the Arctic Ocean. Geophys Res
711 Lett 38, n/a-n/a.
712 Rooney, A.D., Selby, D., Lloyd, J.M., Roberts, D.H., Lückge, A., Sageman, B.B., Prouty, N.G., 2016. Tracking
713 millennial-scale Holocene glacial advance and retreat using osmium isotopes: Insights from the
714 Greenland ice sheet. Quaternary Science Reviews 138, 49-61.
715 Sageman, B.B., Lyons, T.W., Joo, Y.J., 2014a. 9.6 - Geochemistry of Fine-Grained, Organic Carbon-Rich
716 Facies A2 - Holland, Heinrich D, in: Turekian, K.K. (Ed.), Treatise on Geochemistry (Second
717 Edition). Elsevier, Oxford, pp. 141-179.
718 Sageman, B.B., Singer, B.S., Meyers, S.R., Siewert, S.E., Walaszczyk, I., Condon, D.J., Jicha, B.R.,
719 Obradovich, J.D., Sawyer, D.A., 2014b. Integrating Ar-40/Ar-39, U-Pb, and astronomical clocks in
720 the Cretaceous Niobrara Formation, Western Interior Basin, USA. Geological Society of America
721 Bulletin 126, 956-973.
722 Scholle, P.A., Arthur, M.A., 1980. Carbon isotope fluctuations in Cretaceous pelagic limestones -
723 potential stratigraphic and petroleum exploration tool. AAPG Bulletin 64, 67-87.
724 Scott, C., Lyons, T.W., 2012. Contrasting molybdenum cycling and isotopic properties in euxinic versus
725 non-euxinic sediments and sedimentary rocks: Refining the paleoproxies. Chemical Geology 324,
726 19-27.
727 Selby, D., Creaser, R.A., 2003. Re-Os geochronology of organic rich sediments: an evaluation of organic
728 matter analysis methods. Chemical Geology 200, 225-240.
729 Talbot, M. R., 1990, A review of the palaeohydrological interpretation of carbon and oxygen isotopic
730 ratios in primary lacustrine carbonates: Chemical Geology: Isotope Geoscience section, v. 80, no.
731 4, p. 261-279.
732 Talbot, M.R., Jensen, N.B., Lærdal, T. and Filippi, M.L., 2006. Geochemical responses to a major
733 transgression in giant African lakes. Journal of Paleolimnology 35, 467-489.
734 Tessin, A., Hendy, I., Sheldon, N., Sageman, B., 2015. Redox-controlled preservation of organic matter
735 during “OAE 3” within the Western Interior Seaway. Paleoceanography 30, 702-717.
736 Tribovillard, N., Algeo, T.J., Lyons, T., Riboulleau, A., 2006. Trace metals as paleoredox and
737 paleoproductivity proxies: An update. Chemical Geology 232, 12-32.

738 Turgeon, S.C., Creaser, R.A., 2008. Cretaceous oceanic anoxic event 2 triggered by a massive magmatic
739 episode. Nature 454, 323-U329.
740 Wagreich, M., 2012. "OAE 3" - regional Atlantic organic carbon burial during the Coniacian-Santonian.
741 Climate of the Past 8, 1447-1455.
742 Wan, X., Zhao, J., Scott, R.W., Wang, P., Feng, Z., Huang, Q., Xi, D., 2013. Late Cretaceous stratigraphy,
743 Songliao Basin, NE China: SK1 cores. Palaeogeography Palaeoclimatology Palaeoecology 385, 31-
744 43.
745 Wang, C.S., Feng, Z.G., Zhang, L.M., Huang, Y.J., Cao, K., Wang, P.J., Zhao, B., 2013. Cretaceous
746 paleogeography and paleoclimate and the setting of SKI borehole sites in Songliao Basin,
747 northeast China. Palaeogeography Palaeoclimatology Palaeoecology 385, 17-30.
748 Wang, P.J., Gao, Y., Cheng, R., Wang, G., Wu, H., Wan, X., Yang, G., Wang, Z., 2009. Description of
749 Cretaceous Sedimentary Sequence of the Second and Third Member of the Qingshankou
750 Formation Recovered by CCSD-SK-Is Borehole in Songliao Basin: Lithostratigraphy, Sedimentary
751 Facies and Cyclic Stratigraphy. Earth Science Frontiers 16, 288-313.
752 Wang, P.J., Mattern, F., Didenko, N.A., Zhu, D.F., Singer, B., Sun, X.M., 2016a. Tectonics and cycle system
753 of the Cretaceous Songliao Basin: An inverted active continental margin basin. Earth-Science
754 Reviews 159, 82-102.
755 Wang, T., Ramezani, J., Wang, C., Wu, H., He, H., Bowring, S.A., 2016b. High-precision U–Pb
756 geochronologic constraints on the Late Cretaceous terrestrial cyclostratigraphy and
757 geomagnetic polarity from the Songliao Basin, Northeast China. Earth Planet Sc Lett 446, 37-44.
758 Wedepohl, K.H., 1971. Environmental influences on the chemical composition of shales and clays.
759 Physics and Chemistry of the Earth 8, 307-333.
760 Wendler, I., 2013. A critical evaluation of carbon isotope stratigraphy and biostratigraphic implications
761 for Late Cretaceous global correlation. Earth-Science Reviews 126, 116-146.
762 Wu, H., Zhang, S., Jiang, G., Hinnov, L., Yang, T., Li, H., Wan, X., Wang, C., 2013. Astrochronology of the
763 Early Turonian-Early Campanian terrestrial succession in the Songliao Basin, northeastern China
764 and its implication for long-period behavior of the Solar System. Palaeogeography
765 Palaeoclimatology Palaeoecology 385, 55-70.
766 Wunsche, L., Gulacar, F.O., Buchs, A., 1987. Several unexpected marine sterols in a fresh-water
767 sediment. Organic Geochemistry 11, 215-219.
768 Xi, D.P., Cao, W.X., Huang, Q.H., Do Carmo, D.A., Li, S., Jing, X., Tu, Y.J., Jia, J.Z., Qu, H.Y., Zhao, J., Wan,
769 X.Q., 2016. Late Cretaceous marine fossils and seawater incursion events in the Songliao Basin,
770 NE China. Cretaceous Research 62, 172-182.
771 Xu, W., Ruhl, M., Jenkyns, H.C., Hesselbo, S.P., Riding, J.B., Selby, D., Naafs, B.D.A., Weijers, J.W.H.,
772 Pancost, R.D., Tegelaar, E.W., Idiz, E.F., 2017. Carbon sequestration in an expanded lake system
773 during the Toarcian oceanic anoxic event. Nature Geosci advance online publication.
774 Yang, Y.T., 2013. An unrecognized major collision of the Okhotomorsk Block with East Asia during the
775 Late Cretaceous, constraints on the plate reorganization of the Northwest Pacific. Earth-Science
776 Reviews 126, 96-115.
777 Zhao, J., Wan, X.Q., Xi, D.P., Jing, X., Li, W., Huang, Q.H., Zhang, J.Y., 2014. Late Cretaceous palynology
778 and paleoclimate change: Evidence from the SK1 (South) core, Songliao Basin, NE China. Sci.
779 China-Earth Sci. 57, 2985-2997.

Figure1

Click here to download Figure: Fig1.pdf

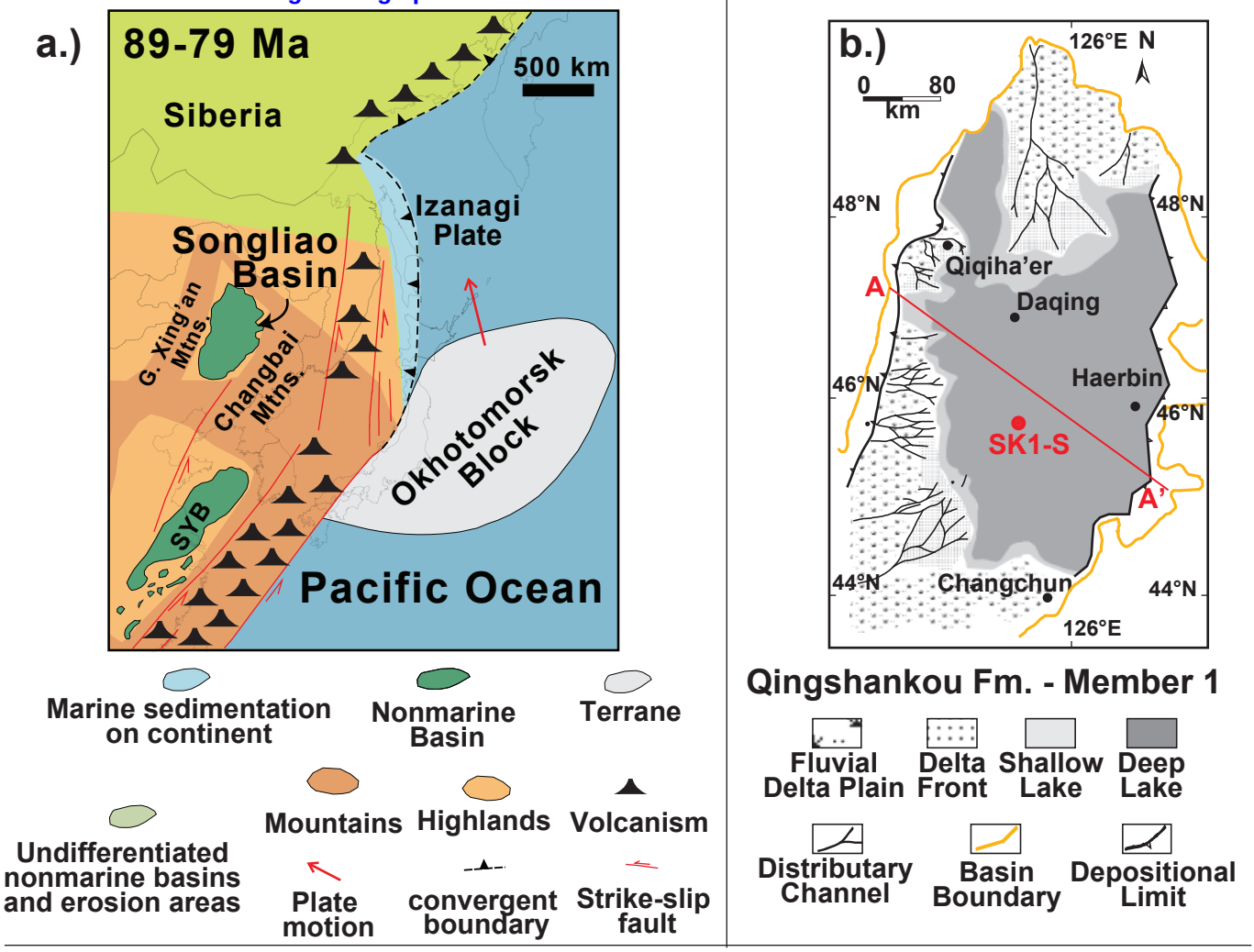

Figure2

Click here to download Figure: Fig2.pdf

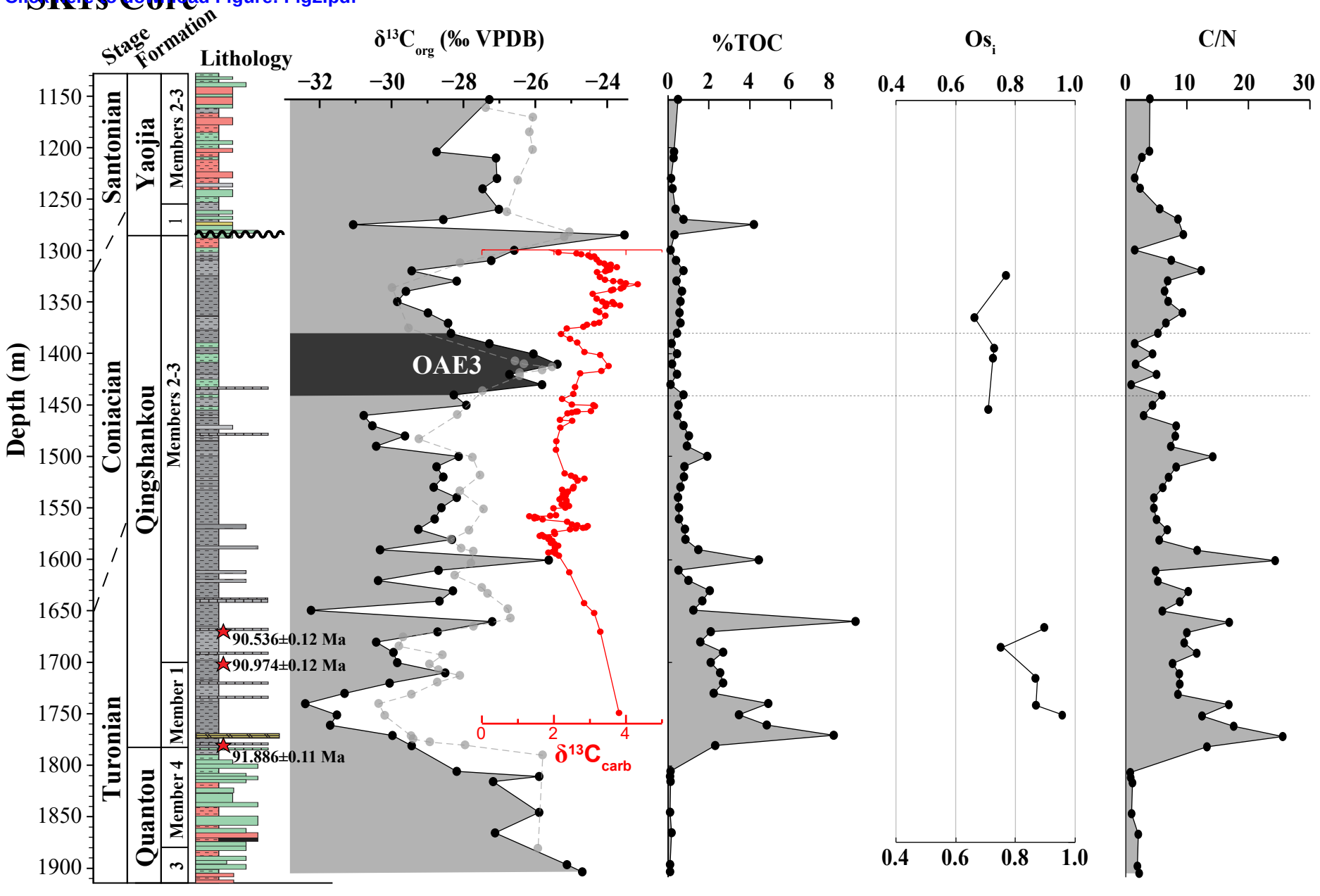

Figure3

Click here to download Figure: Fig3.pdf

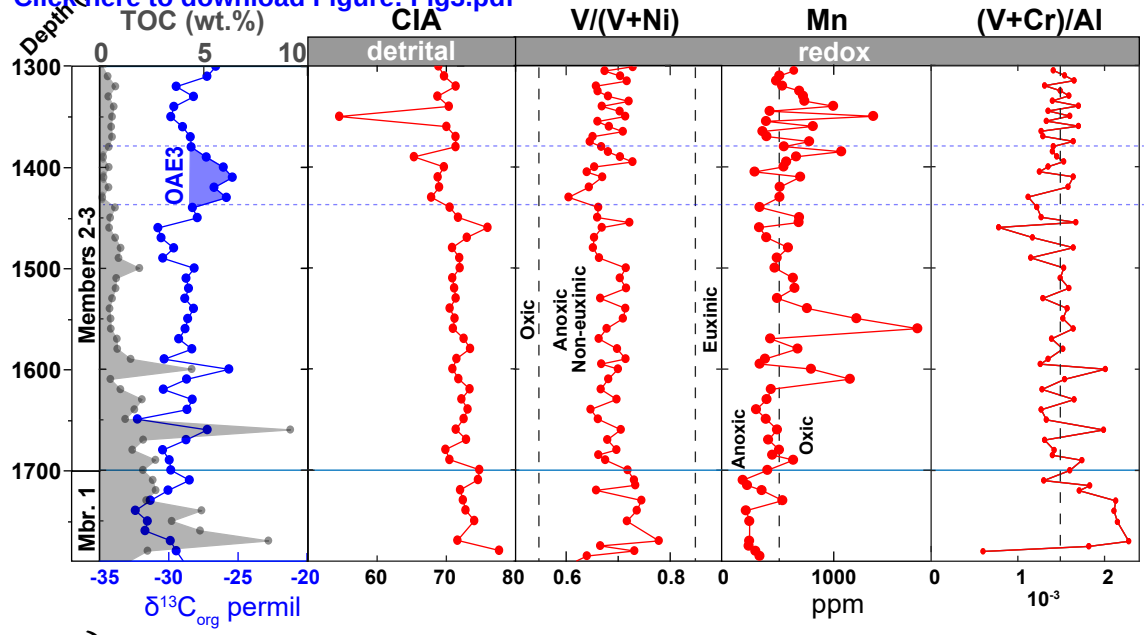

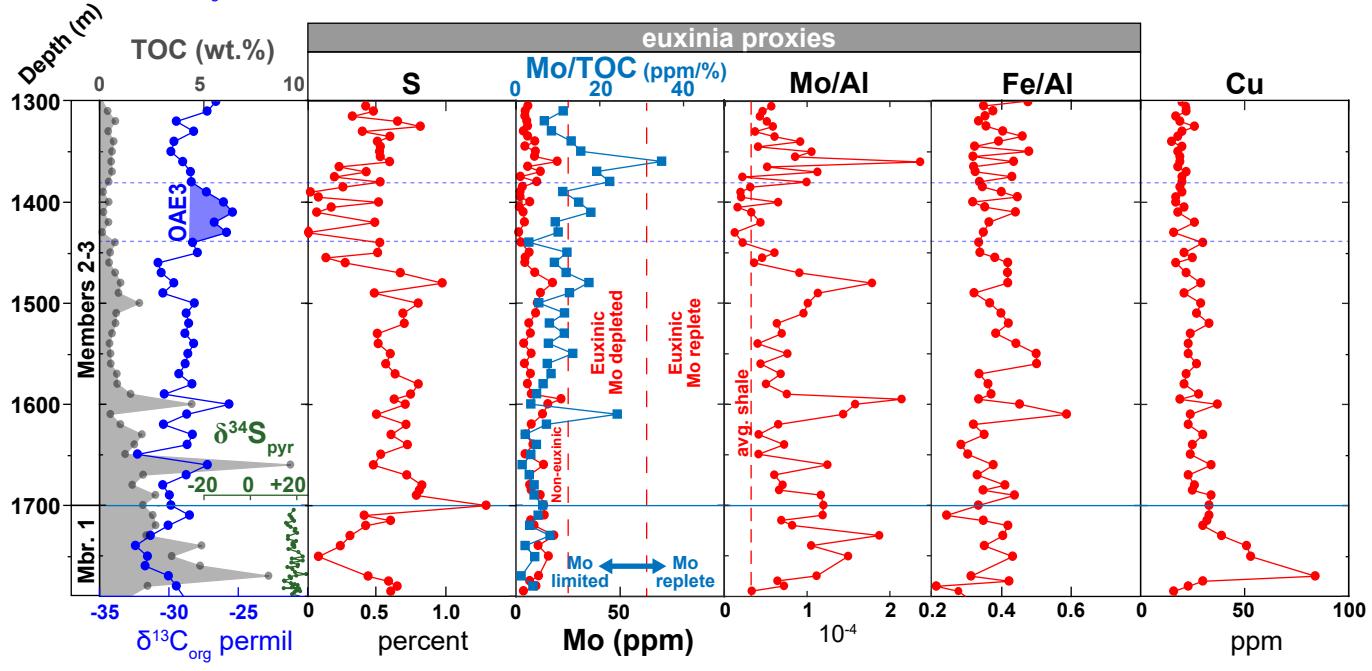

Figure4

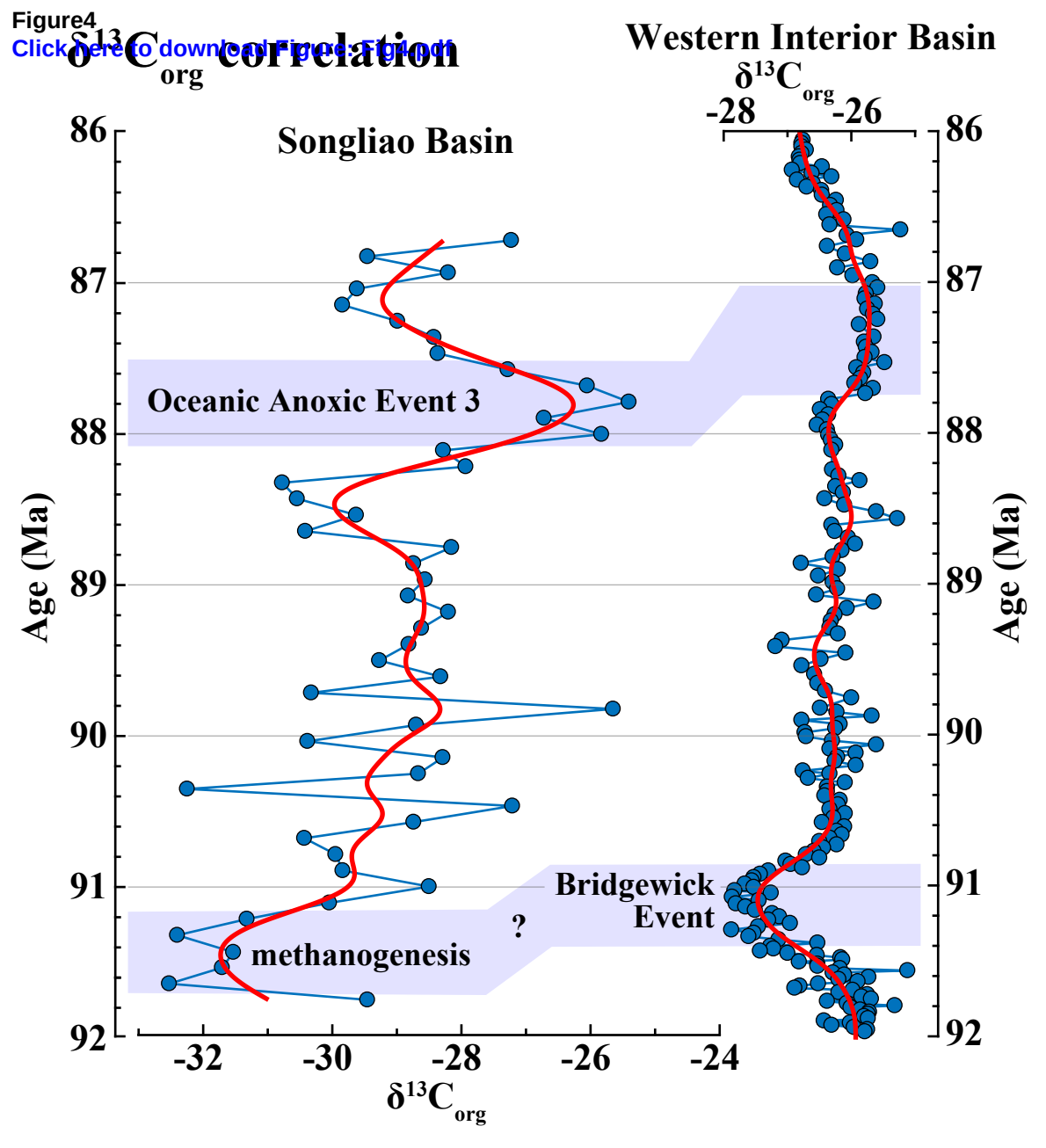

Figure5

Click here to download Figure: Fig5.pdf

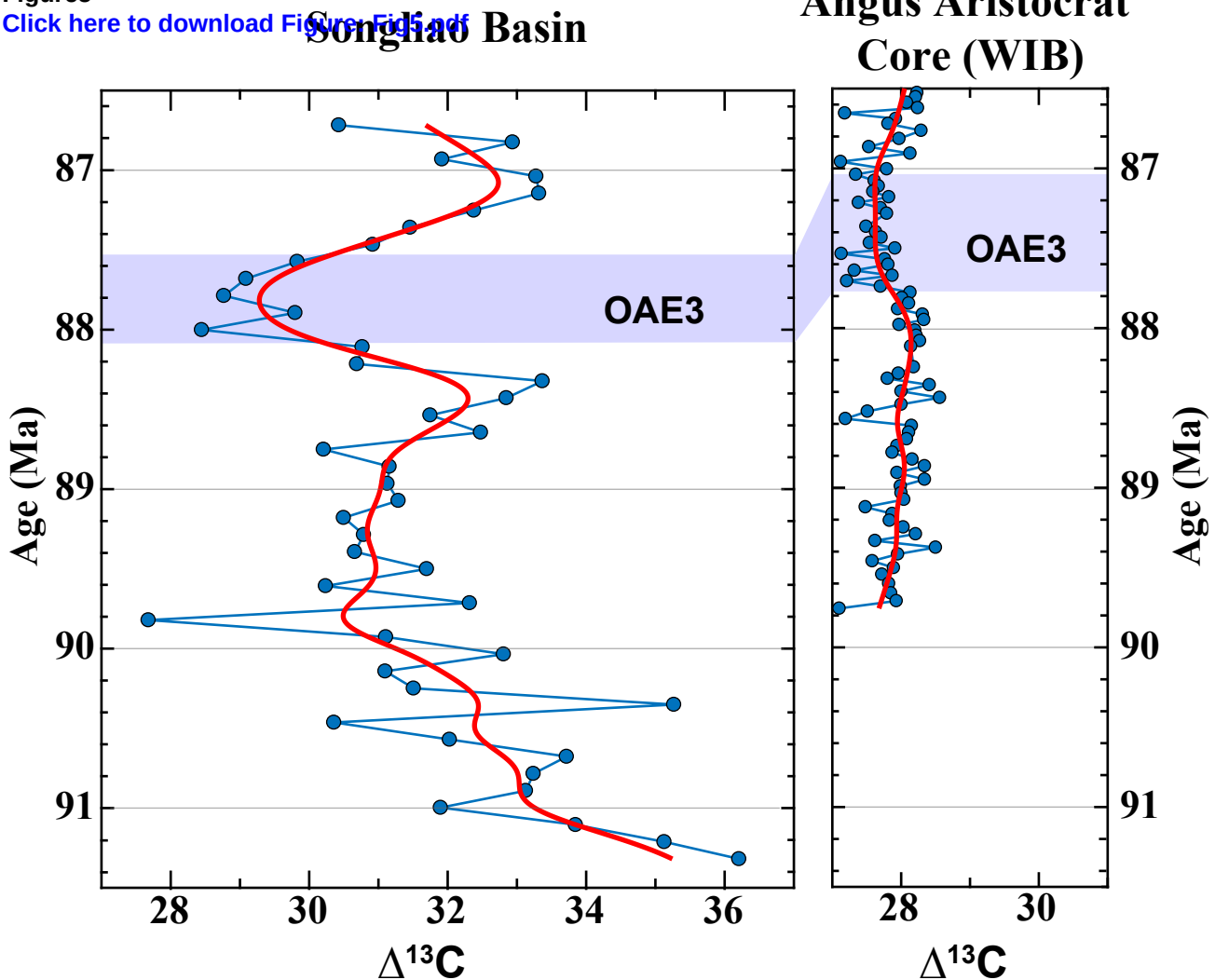

Figure6

Click here to download Figure: Fig6.pdf

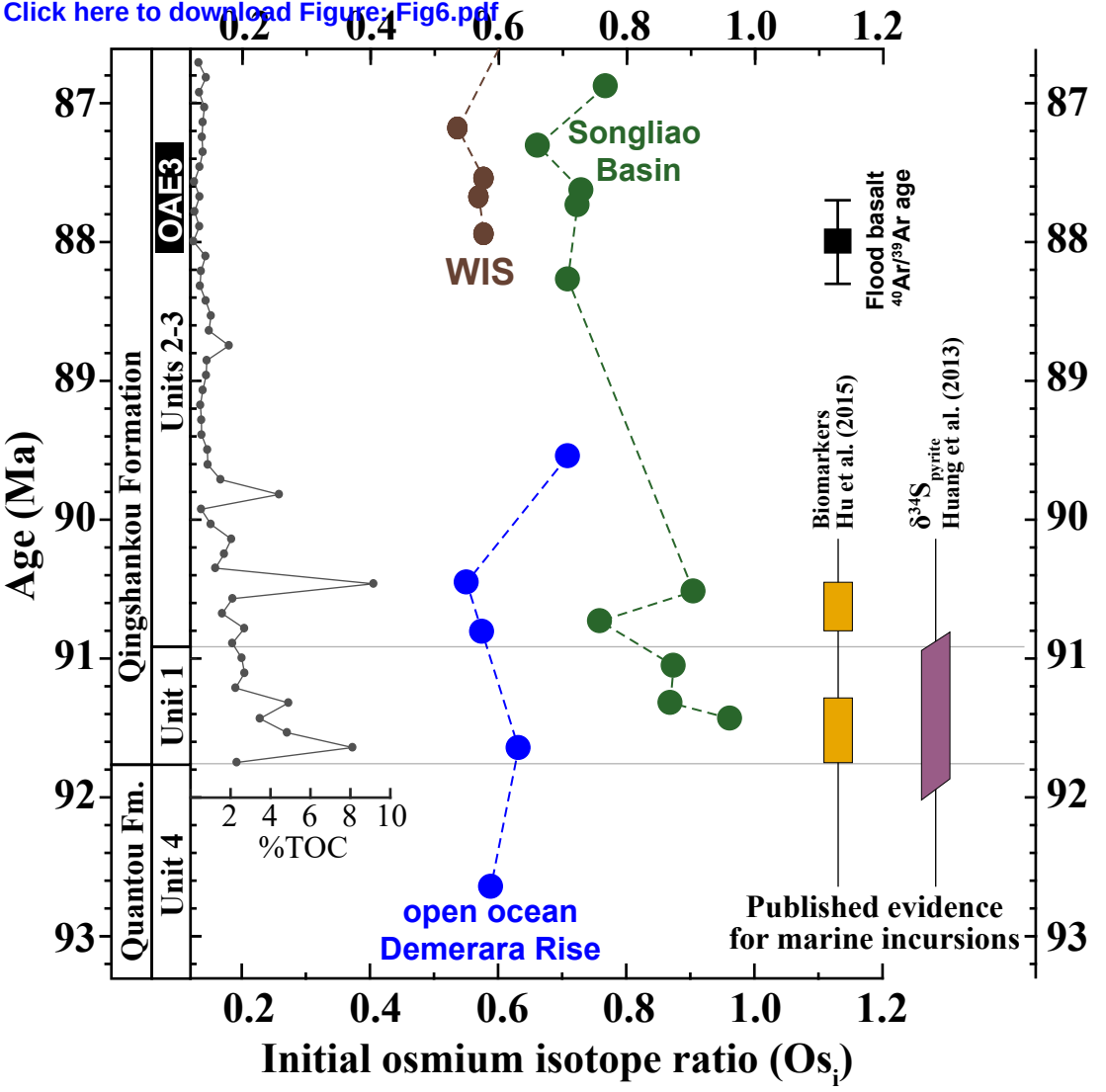

Figure7

Click here to download Figure: Fig7.pdf

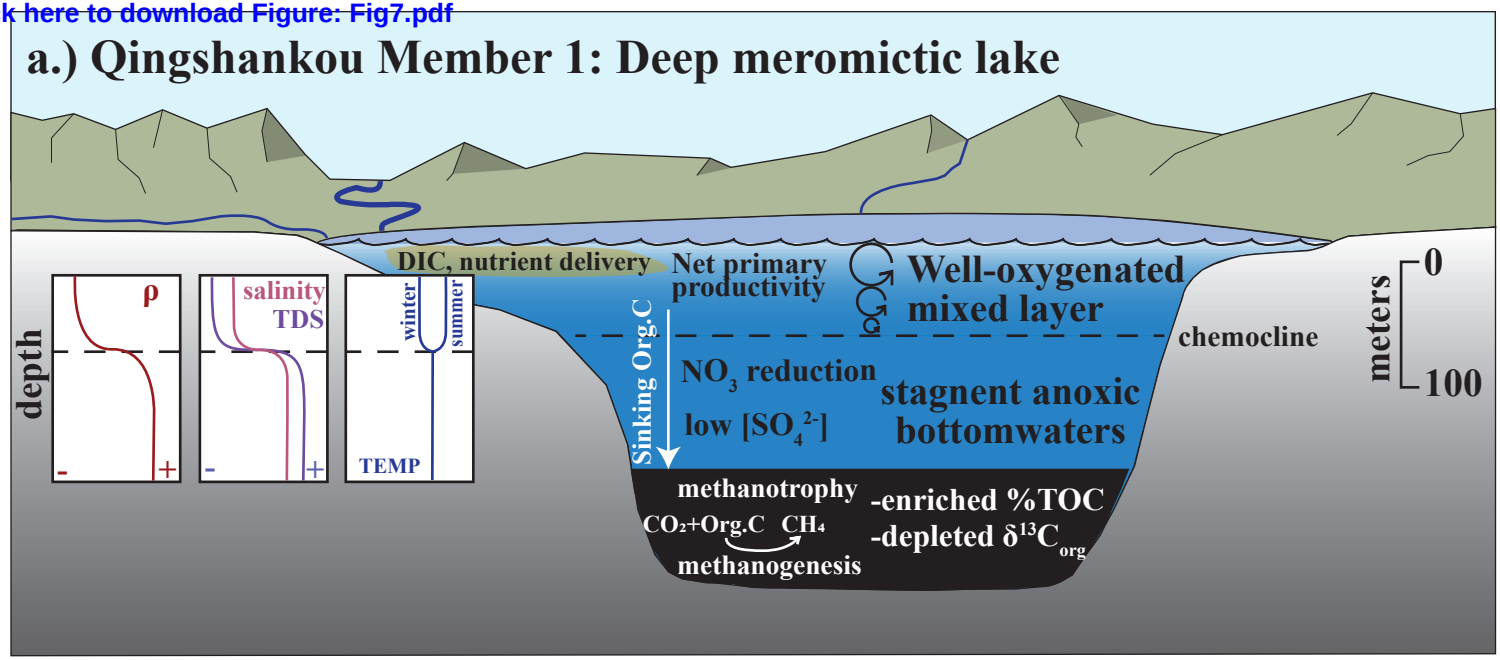

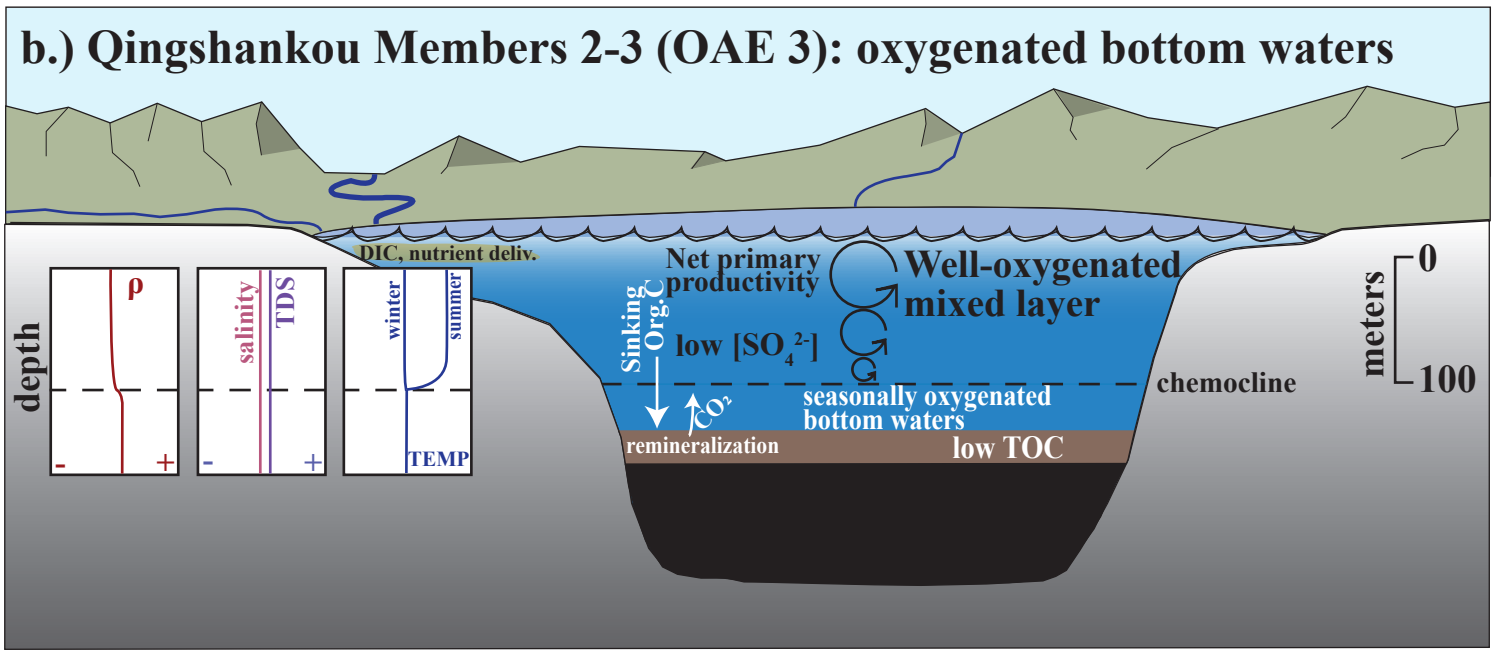

Revised appendix

Click here to download Supplementary material for online publication only: Jonesetal_Appendix_revised.docx

Supplementary material table A1

Click here to download Supplementary material for online publication only: AppendixTable1_GeochemData.xlsx

Supplementary material table A2

Click here to download Supplementary material for online publication only: AppendixTable2_XRFdata.xlsx